Automotive Experiences
Vol. 4 No.3 (2021) pp. 119-130
p-ISSN: 2615-6202 e-ISSN: 2615-6636

Research Paper

# Aerodynamics of Bus Platooning under Crosswind

**Aan Yudianto**[1], **I Wayan Adiyasa**[2], **Afri Yudantoko**[1,3]

[1] Automotive Design Laboratory, Department of Automotive Engineering Education, Universitas Negeri Yogyakarta, 55281, Indonesia
[2] Autotronic Laboratory, Department of Automotive Engineering Education, Universitas Negeri Yogyakarta, 55281, Indonesia
[3] Technische Universität Dresden, Dresden, 01069, Germany

aan.yudianto@uny.ac.id

https://doi.org/10.31603/ae.5298

Check for updates

Published by Automotive Laboratory of Universitas Muhammadiyah Magelang collaboration with Association of Indonesian Vocational Educators (AIVE)

*Article Info*
*Submitted:* 18/07/2021
*Revised:* 04/08/2021
*Accepted:* 05/08/2021
*Online first:* 08/09/2021

## Abstract

The aerodynamic benefits of a vehicle in a platoon could be distracted by an imposed crosswind on it. The study aims to investigate the alteration of aerodynamic coefficient comprising drag force coefficient, lift force coefficient, side force coefficient, and pressure coefficient of buses traveling in a platoon by considering crosswind. A Computational Fluid Dynamic (CFD) simulation was carried out on a detailed bus model. Proposed meshing techniques were also offered. The investigation considered the yaw angle from 0° to 30° and inter-bus distances by proposed coefficient X/L from 0.05 to 1.25. The results in the changes in the aerodynamic performance of both buses were presented. The advantages of platoon configuration were described in more detail when no crosswind was considered in terms of the generated turbulence kinetic energy of the leading and following bus. The results indicated that a crosswind deteriorates aerodynamic benefits during the platoon. The inter-bus distance determines how the airflow around the bus behaves, leading to the variation in aerodynamic advantages experienced by buses. Comparison between the numerical study and experiment indicated a satisfactory correlation of results validation.

**Keywords:** Aerodynamics; Bus; CFD; Convoy; Crosswind; Platoon; Yaw angle

## 1. Introduction

Several vehicles orderly travels in a coordinated manner which has a leading vehicle that the action is followed by other following vehicles is a broad definition of vehicle platooning investigated in this study. Platooning vehicles, sometimes called vehicles traveling in convoy, have gathered increasing attention and become a strategy to reduce vehicle fuel consumption and support green mobility movements [1]. The reduction of drag force on a vehicle leads to a reduction in overall vehicle resistance. Thus, the fuel efficiency of a vehicle is improved due to less power required by the engine leading the less fuel consumption [2]. This condition leads to the environmental benefits in support of reducing the environmental pollution.

It has been studied that the reducing fuel consumption of a vehicle in a platoon was primarily due to the drag reduction benefits from a vehicle platoon configuration. The inter-vehicle distance becomes a main investigated topic by some previous researchers [3]–[6]. It was found that the distance between vehicles becomes the main factor in achieving the aerodynamic advantages of platoon configuration. Some research has also been undertaken to investigate the effect of the external body shape of a vehicle traveling in a platoon [7]–[9]. The external body shape of a vehicle also determines how the air flowing through the body, creating different aerodynamic flow behavior around the vehicle. The rear part of vehicles becomes the main concern since this part determines more in the wake generation behind the vehicle body. The

importance of vehicle platoon configuration also gains more attention to develop machine learning techniques related to predicting the drag force on vehicles in platoon [10]. The proposing technique offers complementary technology to the Computational Fluid Dynamics study to investigate the external aerodynamic effect of vehicles in a platoon.

The fact that vehicles traveling in uncertain environmental conditions, including crosswinds, leads this study to be carried out. The lateral airflow component imposed to a vehicle, unfortunately, increases the side force affecting the vehicle's stability and safety [11]. This effect becomes more vulnerable to a large vehicle. Some studies has been conducted to evaluate the effect of crosswind on large ground vehicle such as a train [12]–[15] and trucks [16]–[19]. The basic concept of aerodynamic behavior of a vehicle subjected to crosswind has also been investigated by using a reference or generic model by some researchers [20]–[23]. The general results indicated that crosswind imposed on a ground vehicle affects the lateral wind component, leading to the elevation of side force coefficient and stability. The resulting wake also increased at some parts of the vehicle's body shape. Previous results indicated that crosswind plays a significant role in distracting aerodynamic benefits of traveling road vehicles.

The previously mentioned study, however, did not extensively investigate the importance of crosswind influence in a group of large vehicles traveling in platoon configuration. This study aims to investigate the aerodynamic response of a large vehicle, which in this case is a bus, in platoon configuration. The investigation includes the case of platooning vehicles without crosswind and with a crosswind. The alteration of the aerodynamic coefficient is extensively explained and including the pressure coefficient around the bus. The results also consider the effect of platooning distance and the visualization of resulting turbulence kinetic energy of a detailed bus model.

## 2. Model Geometry

There has been a number of vehicle models that were employed in automotive aerodynamics ranging from a basic reference model [24] to a complex vehicle model [25]. In this study, a 1/10 scaled and detailed bus model was utilized in the study. The bus model includes a pair of mirrors, the embossed upper part in which the air conditioning compartment was positioned, and the shape representing the wheel of an intercity bus, as depicted in **Figure 1**. The tire of the bus was assumed to have a flat shape, as shown in **Figure 1** Detail A. The door handle, side windshield, and other small detail were excluded for the sake of simplicity. The surface of the underbody was also assumed as a flat surface. The total length (L) of the model was 1,243 mm, the height (H) was 355 mm, and the overall width (W) was 267 mm. The model includes 9° of upper front tapering angle and 5° of rear diffuser angle. However, the wheel compartment was ignored so that the wheel and main body part was merged. The other model dimension was detailed in **Figure 1**.

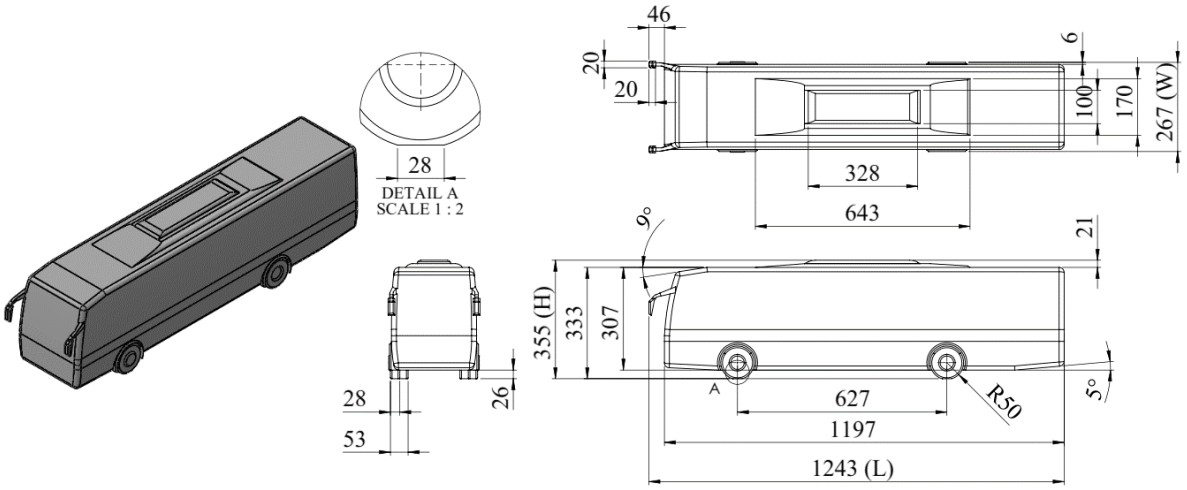


**Figure 1.** Dimension of the detailed bus model

## 3. Computational Domain and Boundary Condition Settings

A cuboid periphery computational domain was selected to perform the simulation. The overall length was 10L, the total height was 5H, and the width was 15W. The leading bus (Bus A) was located at 3L from the inlet 1 boundary. The following bus (Bus B) was positioned depending on the platooning position investigated in this study which was introduced by a coefficient of X/L. A refinement zone was introduced to further investigate in mode detailed mesh around Bus A and Bus B. The size of the refinement zone was 5L in length, 3H in height and 5W in width. The position of this zone was at 2.5L from the inlet 1 boundary, 5W from inlet 2 and outlet 2 boundary. Therefore, the position of the model was exactly at the middle of the computational domain, which is 2W from the side of the refinement zone. Outlet 1 face was also named for the rear face of the computational domain periphery.

Table 1 describes the boundary setting of the computational domain. Since both buses were assumed traveling in +x direction, inlet 1 was set as a velocity-inlet setting that the velocity vector component represents as the velocity of incoming flow ( $v_{if}$) in -x direction, crosswind velocity component ( $v_{cw}$) was also set in +z direction. Instead, the vertical vector component was set to zero. A similar setting was configured at the second inlet face. These settings allowed the simulation to have a resultant velocity produced from the velocity of the incoming flow and crosswind velocity. Outlet 1 and Outlet 2 were set to pressure outlets having atmospheric pressure values to simulate the open area towards both outlet faces. Top and road surfaces were set as slip wall, and both buses surface was no-slip wall setting (see Figure 2).

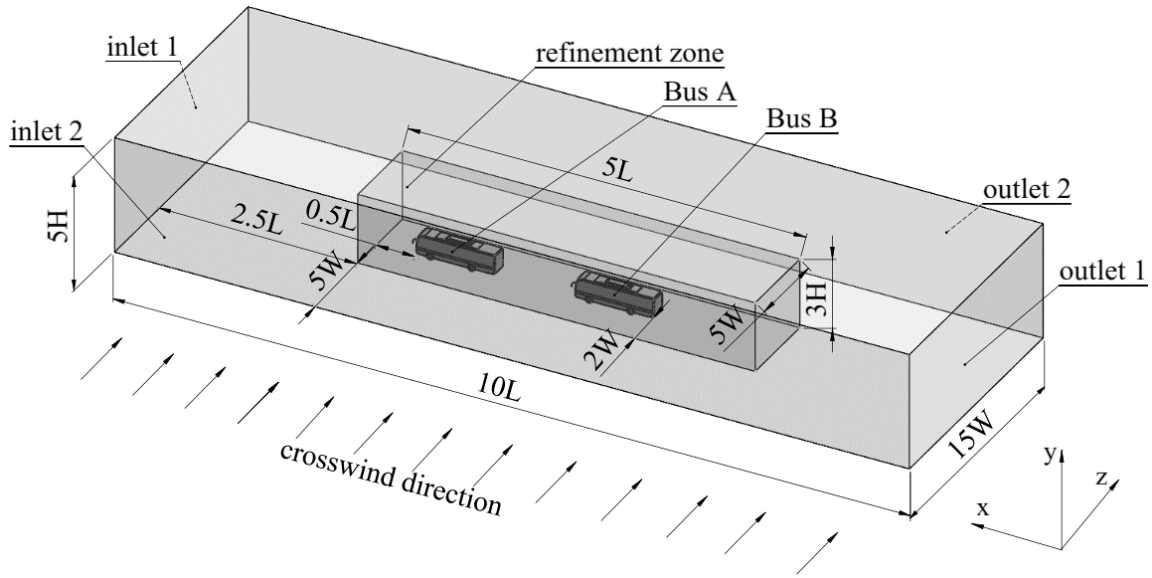


Figure 2. Computational domain

Table 1. Boundary condition settings

| No | Boundary Face | Settings |
|---|---|---|
| 1 | Inlet 1 | Velocity-inlet ( $v_x = v_{if}, v_y = 0, v_z = v_{cw}$) |
| 2 | Inlet 2 | Velocity-inlet ( $v_x = v_{if}, v_y = 0, v_z = v_{cw}$) |
| 3 | Outlet 1 | Pressure-outlet (atmospheric pressure) |
| 4 | Outlet 2 | Pressure-outlet (atmospheric pressure) |
| 5 | Top surface | Slip wall |
| 6 | Road surface | Slip wall |
| 7 | Bus surface | No-slip wall |

## 4. Mesh Strategy

The simulation has been carried out by employing polyhedral mesh. Curvature-based local sizing mesh for both buses was configured with a local minimum size of 0.005 m and a maximum size of 0.3 m. The refinement zone was introduced since the area surrounding the bus was one of the points to be observed. Body-of-influence control type was utilized to set the mesh sizing for refinement zone having 0.05 m target mesh size with 1.2 growth rate. Initially, the surface mesh was generated with a minimum size of 0.05 m and 0.3 m in maximum with a 1.2 growth rate. In this stage, curvature and proximity size function was developed with 18 normal curvature angles. The edges' scope proximity was also set for surface mesh generation. After that, the generation of volume mesh was performed. The smooth transition offset method for volume mesh was generated with triple layers. These 3D mesh settings produce 3,016,812 nodes, 4,085,738 faces with 9,944 edges and 722,915 cells, as portrayed in **Figure 3**. However, this resulting mesh may vary since there are six different platooning configurations. **Figure 3** shows the resulting mesh for one of the platoon configurations. The resulting mesh can be observed that the resulting mesh was detail enough to represent the bus model in this study.

## 5. Platooning Bus Position and Airflow Direction

Six different platooning distances were introduced by means of X/L coefficient and the summation of incoming flow and crosswind generate a certain degree of airflow passing through the buses. The X represents the distance between the bus measured from the rear part of the leading bus to the front windshield of the following bus. The L represents the total length of the bus. The platooning position was investigated at six different positions with X/L equals 0.05, 0.25, 0.50, 0.75, 1.00, and 1.25. The simulation employs a steady simulation, meaning that it kept the position of the following bus unmoved. The velocity of incoming flow ($v_{if}$) was kept at 10 m/s in -x direction. Different yaw angles ($\alpha$) with $\alpha = 0, \alpha = 10, \alpha = 20$, and $\alpha = 30$, were performed to simulate the platooning bus in different wind directions. These angles resulted from the velocity vector resultant of the velocity of incoming flow ($v_{if}$) and crosswind velocity ($v_{cw}$). In this case, the crosswind velocity direction was in +z of the axis. Therefore, the expression of resultant velocity ($v_{res}$) is written in Equation (1), and the yaw angle ($\alpha$) can be calculated as expressed by Equation (2). **Figure 4** portrays the schematic of bus position and airflow direction.

$$v_{res} = \sqrt{v_{if}^2 + v_{cw}^2} \quad (1)$$

$$\alpha = arc\ \tan\left(\frac{v_{cw}}{v_{if}}\right) \quad (2)$$

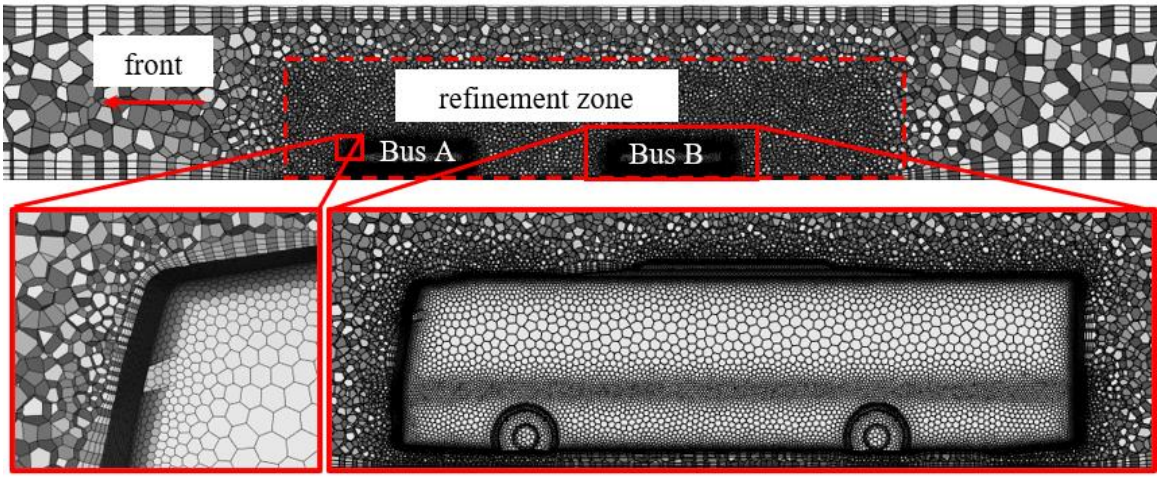


**Figure 3.** Mesh strategy

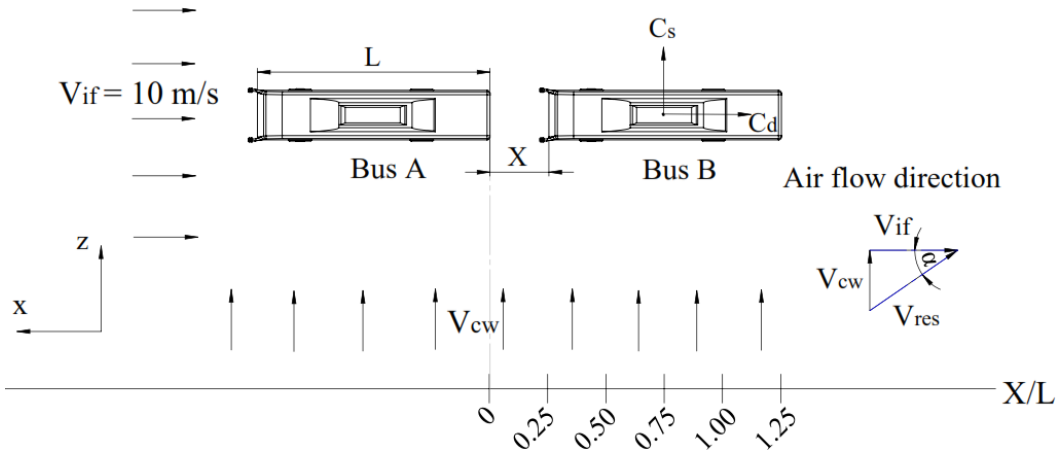


**Figure 4.** Bus position and airflow direction

## 6. Aerodynamic Parameter Definition

This study was undertaken to assess the changes of aerodynamic forces coefficient together with turbulence kinetic energy of two buses in a platoon with a certain distance by considering the wind perpendicular to the bus motion. The aerodynamic forces coefficient investigated in this study includes drag coefficient ($C_d$), side force coefficient ($C_s$), lift force coefficient ($C_l$) and pressure coefficient $(C_p)$ that mathematically is expressed in Equation (5) to (8).

$$C_d = \frac{F_D}{\frac{1}{2}\rho v_{res}^2 A} \quad (5)$$

$$C_s = \frac{F_s}{\frac{1}{2}\rho v_{res}^2 A} \quad (6)$$

$$C_l = \frac{F_l}{\frac{1}{2}\rho v_{res}^2 A} \quad (7)$$

$$C_p = \frac{p - p_{if}}{\frac{1}{2}\rho v_{if}^2} \quad (8)$$

The drag force, side force and lift force experienced by bus is denoted as $F_D$, $F_s$, and $F_l$ respectively in Equation (5), (6) and (7). Those three forces are divided by half of the product of air density (ϱ), a square of resultant velocity ($v_{res}$) and bus projected area ($A$). The term $p$ and $p_{if}$ in Equation (8) represent the static pressure in the evaluated area and static pressure in the free stream respectively. Moreover, the $v_{if}$ is the incoming flow velocity. Another aerodynamic parameter evaluated in this study is the turbulence kinetic energy $(k)$ that is defined as half of the total square of the standard deviation of each airflow velocity component of each axis represented by $u, v$ and $w$ in Equation (9).

$$k = \frac{1}{2}\left(\overline{(u')^2} + \overline{(v')^2} + \overline{(w')^2}\right) \quad (9)$$

## 7. Results and Discussion

### 7.1. *Alteration of aerodynamic coefficients*

**Figure 5** compares the changes of drag coefficient of leading and the following bus for each platooning position ranging from X/L = 0.05 to 1.25 by considering yaw angle from $\alpha$ = 0 up to $\alpha$ = 30. As the yaw angle elevates, the value of the drag coefficient also significantly rises, especially for the following bus for a higher distance from the leading bus. The value of the coefficient of drag for the leading bus is hovering at the value of 0.37 up to 0.39 when both buses travel without the interference of crosswind. The value becomes double and triple when crosswind is considered producing yaw angle $\alpha$ = 10 and 30. However, drag coefficient reduction occurs for the leading bus after X/L = 0.25, and it steadily decreases to a value of approximately 0.7 when X/L = 0,75. The value remains for bus distance X/L = 1 and 1.25. A significant alteration of the drag coefficient occurs for Bus B. When X/L is 0.05, drag coefficient values for all yaw angles are between 0.18 to 0.35. As the distance between buses becomes larger, the value for $\alpha$ = 30 significantly increases up to 1.25 for X/L = 1.25. Nevertheless, a quire steady drag coefficient is generated by Bus B for $\alpha$ = 0. The values remain constant after X/L=0.25 to X/L = 1.25, generating drag for a coefficient of approximately 0.23.

The comparison of lift coefficient value alteration between Bus A and Bus B over selected platooning distances is represented in **Figure 6**. A significant upsurge value of lift coefficient can be observed for leading and the following bus. When no crosswind is considered, the leading bus generates downforce having a nearly constant value through all platooning distance

configurations. The value of the lift coefficient rises as the yaw angle elevates for Bus A. The lift coefficient becomes nearly at the highest point of 1.9 at X/L = 0.05. The value goes down constantly to the value around 1.65 from X/L = 0.25 to X/L = 1.25. Nonetheless, Bus B experiences a quite low lift coefficient for X/L up to 0.25. The highest value up to this point is about 0.9 for all yaw angle conditions. The value of lift coefficient, unfortunately, increases as the distance becomes larger for $\alpha$ = 30. Yet, the other values are generally hovering at a similar point for yaw angle less than $\alpha$ = 30.

As it can be expected from the consideration due to the presence of crosswind, the lateral velocity of the wind component increases the value of the lift coefficient. Similar results have also been observed by other studies [26], [27]. The trend is depicted in **Figure 7**. All the side force coefficient values at each yaw angle are generally constant, but when the yaw angle is rising, the values also elevate. The side force coefficient of Bus A reaches the peak of approximately 3.7 at X/L = 0.25. For Bus B, the highest value of side force coefficient undergoes by Bus B when $\alpha$ = 30 at X/L = 1.25 reaching the value of 3.40. This imposed crosswind clearly can deteriorate driving performance of the vehicle [28].

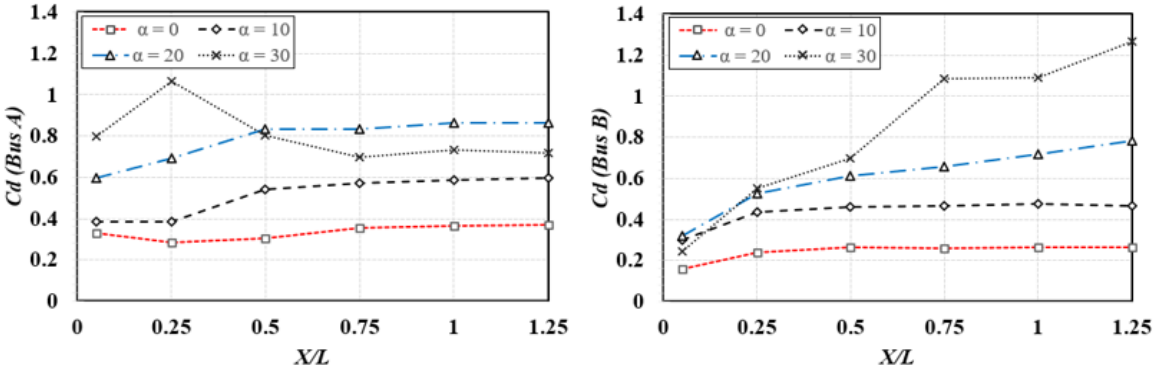


**Figure 5.** Drag force coefficient alteration of bus A and bus B

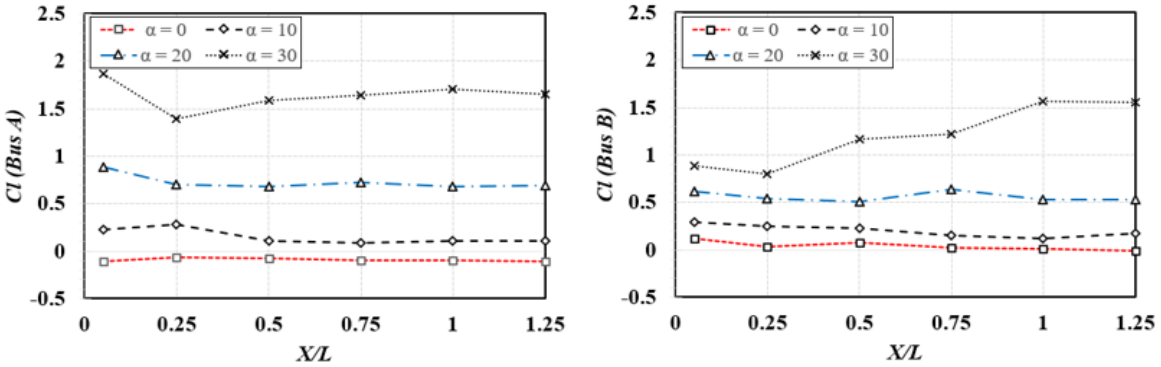


**Figure 6.** Lift force coefficient alteration of bus A and bus B

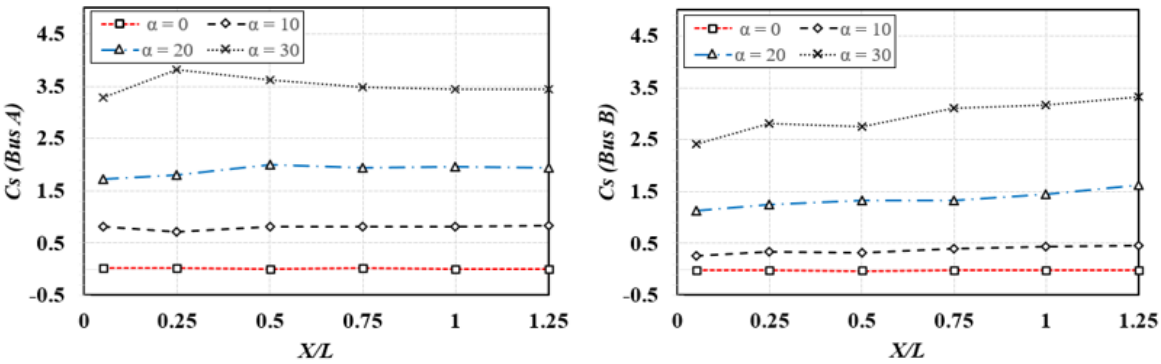


**Figure 7.** Side force coefficient alteration of bus A and bus B

A substantial positive value of pressure coefficient is observed exactly at the front part of the bus in the platoon when $\alpha = 0$, as it is shown in **Figure 8**. The following bus, instead, undergoes a significantly lower value of pressure coefficient at the front part. It is observed that there is nearly zero pressure coefficient when X/L = 0.05 in front of Bus B. The area of the positive value of the pressure coefficient is getting larger as the following bus gets separated from the leading bus. In terms of streamlines contour, the distance of X/L = 0.25 generated a whirlpool utmost located in between both buses. In this condition, the following bus experiences less stagnation point of the incoming flow, and so that surface pressure is small since the airflow direction is sort of hindered by the leading bus. It is investigated with the discussion in the previous point in **Figure 5** that, at the closets position, the following bus benefits more in the aerodynamic drag coefficient, and it lessens when the distance is getting farther.

**Figure 9** to **Figure 11** depict how crosswind affects the pressure coefficient value observed around both buses for all platooning distances. A significant shifting of the positive value of the pressure coefficient is observed when the yaw angle is getting larger. Moreover, a whirlpool starts to generate in the leeward side of the bus model, and the size is indicated larger for large yaw angle imposed to platooning buses. As it can be predicted that the additional lateral velocity component due to crosswind increases the positive value of the pressure coefficient at the surface from which the airstream comes. It is agreed that the side force coefficient grows up when the yaw angle is getting larger, as explained previously in **Figure 7**.

The shortest platooning distance, when X/L = 0.05, creates both buses as if they were merged in to one. As a result, the highest value of pressure coefficient is only undergone by front bus as it is depicted in **Figure 9**(a), **Figure 10**(a) and **Figure 11**(a). The same behavior can be investigated for the whirlpool generation. It is a mere front bus that is generating a whirlpool at the leeward side of the bus. This occurs when $\alpha$ = 10, 20, and 30. As the distance is getting larger, the flow separation occurs, and the airflow starts to flow in between two buses. This can be clearly seen when the platooning distance is X/L=0.50 for $\alpha$ = 20 and 30 (**Figure 10**(c) and **Figure 11**(c)). The characteristic is continuous for larger platooning distances. At high yaw angle, buses in platoon formation that have a large distance have fewer benefits in terms of aerodynamic forces coefficient either for leading or the following bus. These results are proved by **Figure 10**(f) and **Figure 11**(f). The area of pressure coefficient and airflow streamlines are similar for the two buses. Since the airflow direction is far from the side of the bus, the value of the side force coefficient is also similar for both buses. These results support previous researchers examining the pressure coefficient of vehicles in crosswind [29]. These results also agree with the previous results of the side force coefficient previously discussed and portrayed in **Figure 7**.

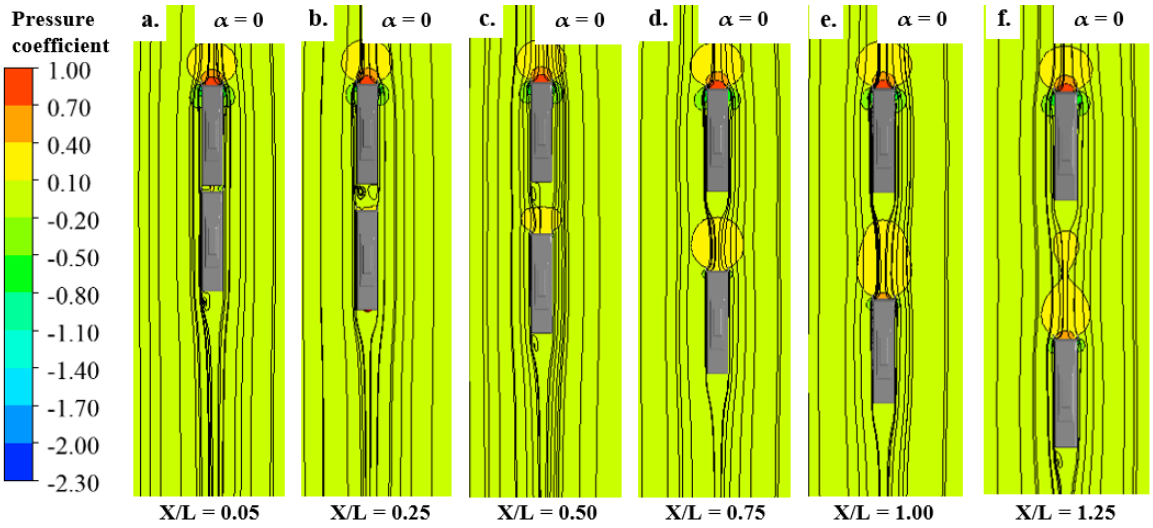


**Figure 8.** Pressure coefficient at $\alpha = 0°$

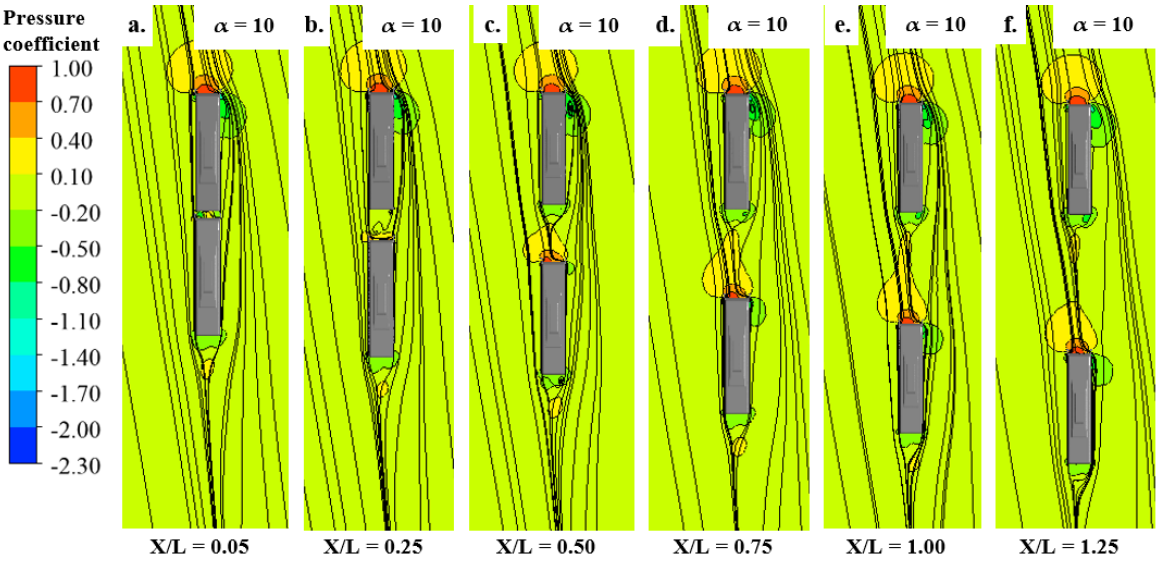


**Figure 9.** Pressure coefficient at $\alpha = 10°$

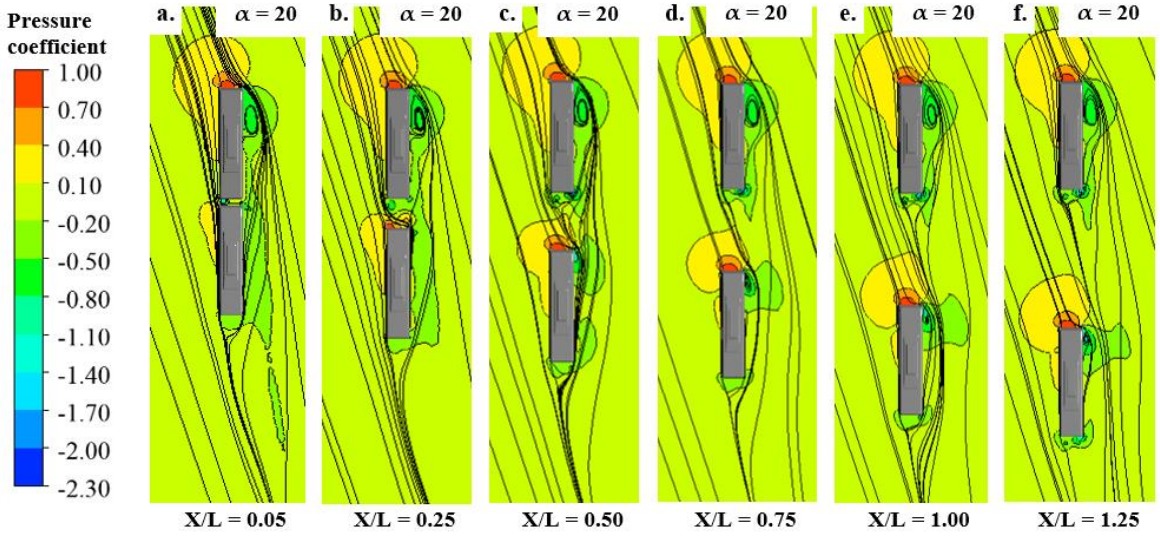


**Figure 10.** Pressure coefficient at $\alpha = 20°$

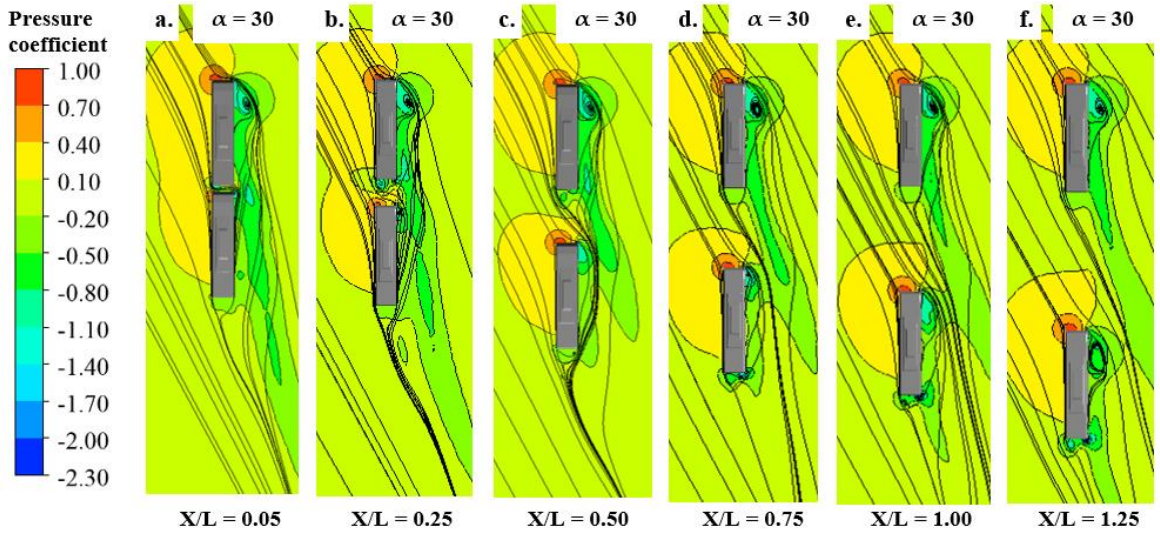


**Figure 11.** Pressure coefficient at $\alpha = 30°$

### 7.2. *Turbulence kinetic energy at* $\alpha = 0°$

The discussion in the previous section indicates that the most beneficial platooning condition happens when the buses travel altogether with the absence of crosswind. This point discusses the turbulence kinetic energy portrayed at the middle vertical plane when the yaw angle $\alpha$ = 0. The comparison of turbulence kinetic energy around the bus is compared in **Figure 12**. The variation of platooning distances causes the different behavior of kinetic energy caused by the air flowing through the vehicle. The assumption used in this study is that it uses a free stream from the front part of the bus model and neglects the induced turbulence from other vehicles or infrastructure around the bus, which can generate a non-uniform and fluctuating airflow [30]. It shifts over the platooning distances. When X/L = 0.05, the highest value of turbulence kinetic energy is located at the top front of the leading bus. Instead, the following bus produces less turbulence kinetic energy. This result agrees with the previous discussion saying that the drag coefficient of Bus B is low at this position. The aerodynamic advantages is experienced by the following bus in terms of drag coefficient and lift coefficient as it is already mentioned and observed in **Figure 5** and **Figure 6**. When X/L equals 0.25, the location of the highest area of turbulence kinetic energy shifts to the tail of the following bus. However, the leading bus also generates turbulence, yet the value is less than the following bus. With the higher platooning distances, which are from X/L = 0.50 to 1.25, the turbulence kinetic energy value reaches the highest point located at the tail of the leading bus. At this point, it can be observed that the airflow is then continued to the following bus through the upper part of the bus. The following bus also generates turbulence, but the value is less than the leading bus.

## 8. Validation of Numerical Simulation

The results discussed in this study were validated by comparing the results from the current simulation and the real experiment using wind tunnel conducted by Meile et al. [31], which also agrees with the result of Ahmed et al.'s original Ahmed Body reference model [32]. An Ahmed Body with a rear slant angle 25° reference model was utilized in this study to perform simulation which then compared to the experimental results. Two aerodynamic coefficient results on the current simulation, drag coefficient and lift coefficient, are selected to be then compared to the experimental results. The percentage of differences is then calculated by Equation (10).

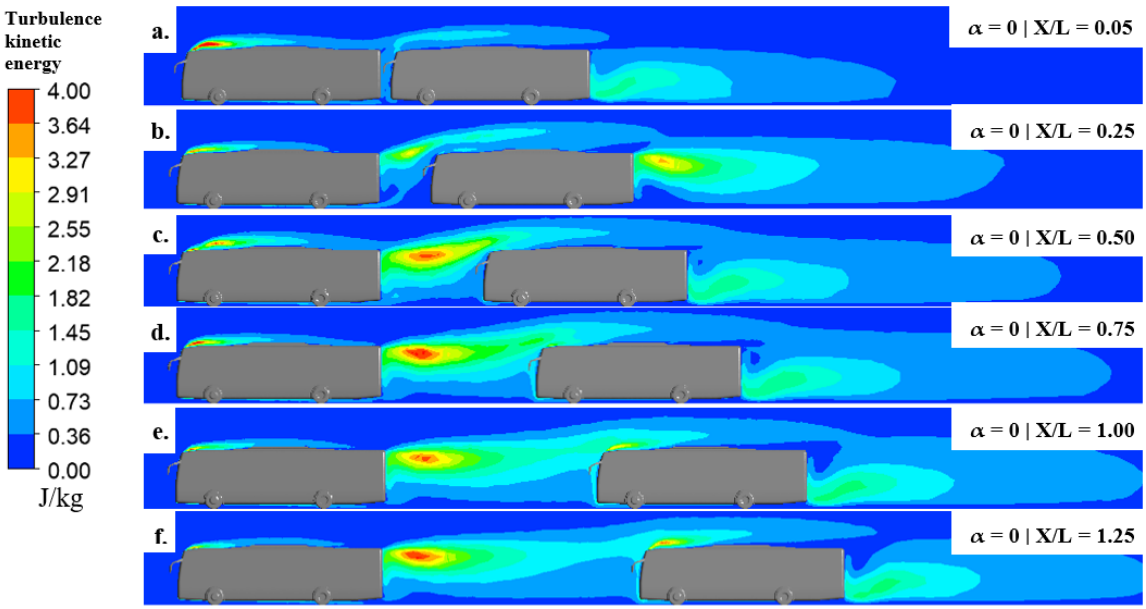


**Figure 12.** Turbulence kinetic energy of bus platooning at $\alpha = 0°$ captured at vertical midplane.

$$\%\ of\ Difference = \left(\frac{Experimental\ Results - Simulation\ Results}{Experimental\ Results}\right) \cdot 100 \qquad (10)$$

**Figure 13** shows the comparison of the drag and lift coefficient for both current simulation in this study and experiment by Meile et al. [31]. The present simulation obtained the resulting drag coefficient of 0.298 and lift coefficient of 0.355, while the experimental validation resulted in 0.299 and 0.345 of drag coefficient and lift coefficient, respectively. Therefore, the resulting different percentage of drag force coefficient is 0.37%, and the lift force coefficient is 2.90%. A satisfactory correlation between the numerical simulation and experiment has been achieved, and the results in this study have been well validated.

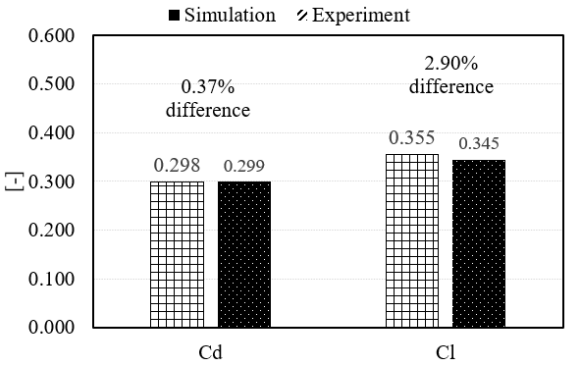


**Figure 13.** Comparison of drag and lift coefficient between simulation and experiment.

## 9. Conclusion

The study has been carried out to investigate the aerodynamic benefits of two detailed bus scaled models traveling in platoon formation in the case of considered crosswind. A platooning bus formation brings aerodynamic benefits depending on the distance between buses. However, the presence of a large crosswind, producing a large number of yaw angles, significantly reduces the aerodynamic advantages of platoon formation. In this case, the following bus obtains more benefits as opposed to the leading bus, indicated by reducing the value of generated drag coefficient in the small distance between buses when $\alpha$ = 0. These benefits are reduced as the yaw angle produced by crosswind increases. Moreover, the larger distance between buses also generates a higher value of turbulence kinetic energy that reduces the aerodynamic benefit of buses. Future works potentially to be performed are the assessment of reliability analysis of vehicles in platoon since it has been studied that a platooning formation brings convinced advantages in certain cases. A dynamic simulation is also required to consider the shift of the center of gravity of the bus during acceleration or turning [33] since it may affect the position of one bus to another.

## Acknowledgement

This work was the branch of the research undertaken by Automotive Engineering Education Department Research Group 2021 that was fully funded by Universitas Negeri Yogyakarta under the full support of Automotive Design Laboratory - Department of Automotive Engineering Education and CAD Laboratory - Department of Mechanical Engineering Education for licensed software. Appreciations are expressed to Professors, lecturers, and students involved in this research.

## Author's Declaration

### Authors' contributions and responsibilities

The authors made substantial contributions to the conception and design of the study. The authors took responsibility for data analysis, interpretation and discussion of results. The authors read and approved the final manuscript.

### Funding

No funding information from the authors.

### Availability of data and materials

All data are available from the authors.

### Competing interests

The authors declare no competing interest.

### Additional information

No additional information from the authors.

## References

[1] A. Davila, E. Del Pozo, E. Aramburu, and A. Freixas, "Environmental benefits of vehicle platooning," in *SAE Technical Papers*, 2013, doi: 10.4271/2013-26-0142.

[2] A. Davila and M. Nombela, "Platooning-safe and eco-friendly mobility," in *SAE Technical Papers*, 2012, doi: 10.4271/2012-01-0488.

[3] J. Törnell, S. Sebben, and D. Söderblom, "Influence of Inter-Vehicle Distance on the Aerodynamics of a Two-Truck Platoon," *International Journal of Automotive Technology*, 2021, doi: 10.1007/s12239-021-0068-5.

[4] S. T. Kaluva, A. Pathak, and A. Ongel,

"Aerodynamic drag analysis of autonomous electric vehicle platoons," *Energies*, 2020, doi: 10.3390/en13154028.

[5] C. H. Bruneau, K. Khadra, and I. Mortazavi, "Flow analysis of square-back simplified vehicles in platoon," *International Journal of Heat and Fluid Flow*, 2017, doi: 10.1016/j.ijheatfluidflow.2017.05.008.

[6] B. R. McAuliffe and M. Ahmadi-Baloutaki, "A Wind-Tunnel Investigation of the Influence of Separation Distance, Lateral Stagger, and Trailer Configuration on the Drag-Reduction Potential of a Two-Truck Platoon," *SAE International Journal of Commercial Vehicles*, 2018, doi: 10.4271/02-11-02-0011.

[7] Q. Li, W. Dai, Z. Yang, and Q. Jia, "Investigation on aerodynamic characteristics of tailing vehicle hood in a two-vehicle platoon," *Proceedings of the Institution of Mechanical Engineers, Part D: Journal of Automobile Engineering*, 2020, doi: 10.1177/0954407019857430.

[8] G. Le Good, M. Resnick, P. Boardman, and B. Clough, "An investigation of aerodynamic effects of body morphing for passenger cars in close-proximity," *Fluids*, 2021, doi: 10.3390/fluids6020064.

[9] B. Q. He, Y. Z. Wu, and L. M. Fu, "Influence of vehicle shape on the aerodynamic characteristics of intelligent vehicle platoon," *Jilin Daxue Xuebao (Gongxueban)/Journal of Jilin University (Engineering and Technology Edition)*, 2008.

[10] F. Jaffar, T. Farid, M. Sajid, Y. Ayaz, and M. J. Khan, "Prediction of Drag Force on Vehicles in a Platoon Configuration Using Machine Learning," *IEEE Access*, 2020, doi: 10.1109/ACCESS.2020.3035318.

[11] H. Sun, E. Karadimitriou, X. M. Li, and D. Mathioulakis, "Aerodynamic Interference between Two Road Vehicle Models during Overtaking," *Journal of Energy Engineering*, 2019, doi: 10.1061/(asce)ey.1943-7897.0000601.

[12] E. Deng *et al.*, "Aerodynamic response of high-speed trains under crosswind in a bridge-tunnel section with or without a wind barrier," *Journal of Wind Engineering and Industrial Aerodynamics*, 2021, doi: 10.1016/j.jweia.2020.104502.

[13] T. Li, D. Qin, and J. Zhang, "Effect of RANS Turbulence Model on Aerodynamic Behavior of Trains in Crosswind," *Chinese Journal of Mechanical Engineering (English Edition)*, 2019, doi: 10.1186/s10033-019-0402-2.

[14] Z. Guo *et al.*, "Numerical study for the aerodynamic performance of double unit train under crosswind," *Journal of Wind Engineering and Industrial Aerodynamics*, 2019, doi: 10.1016/j.jweia.2019.06.014.

[15] J. Niu, D. Zhou, and X. Liang, "Numerical investigation of the aerodynamic characteristics of high-speed trains of different lengths under crosswind with or without windbreaks," *Engineering Applications of Computational Fluid Mechanics*, 2018, doi: 10.1080/19942060.2017.1390786.

[16] F. Chen, H. Peng, X. Ma, J. Liang, W. Hao, and X. Pan, "Examining the safety of trucks under crosswind at bridge-tunnel section: A driving simulator study," *Tunnelling and Underground Space Technology*, 2019, doi: 10.1016/j.tust.2019.103034.

[17] F. Chen, H. Peng, X. Ma, J. Liang, and X. Pan, "Model of Driving Behavior of Truck Driver Under Crosswind," *Tongji Daxue Xuebao/Journal of Tongji University*, 2020, doi: 10.11908/j.issn.0253-374x.19325.

[18] X. J. Hu, P. Y. Ding, P. Qin, P. Guo, W. Bin Luo, and B. Yang, "Numerical simulation on aerodynamic characteristics of heavy-duty truck driving on bridge within crosswind," *Jilin Daxue Xuebao (Gongxueban)/Journal of Jilin University (Engineering and Technology Edition)*, 2012.

[19] X. J. Hu, P. Qin, L. Liao, P. Guo, J. Y. Wang, and B. Yang, "Numerical simulation of the aerodynamic characteristics of heavy-duty trucks through viaduct in crosswind," *Journal of Hydrodynamics*, 2014, doi: 10.1016/S1001-6058(14)60044-5.

[20] I. A. Ishak, M. S. Mat Ali, M. F. Mohd Yakub, and S. A. Z. Shaikh Salim, "Effect of crosswinds on aerodynamic characteristics around a generic train model," *International*

*Journal of Rail Transportation*, 2019, doi: 10.1080/23248378.2018.1424573.

[21] I. A. Ishak *et al.*, "Aerodynamic characteristics around a generic train moving on different embankments under the influence of crosswind," *Journal of Advanced Research in Fluid Mechanics and Thermal Sciences*, 2019.

[22] H. Li, X. He, H. Wang, S. Peng, S. Zhou, and L. Hu, "Aerodynamics of a two-dimensional bluff body with the cross-section of a train," *Advances in Structural Engineering*, 2020, doi: 10.1177/1369433220921002.

[23] H. Zhu and Y. Zhigang, "Fluid-structure interaction study of three-dimensional vehicle model under crosswind," *Advances in Mechanical Engineering*, 2015, doi: 10.1177/1687814015591318.

[24] G. M. Le Good and K. P. Garry, "On the use of reference models in automotive aerodynamics," in *SAE Technical Papers*, 2004, doi: 10.4271/2004-01-1308.

[25] A. Yudianto, H. A. Susanto, A. Suyanto, I. W. Adiyasa, A. Yudantoko, and N. A. Fauzi, "Aerodynamic performance analysis of open-wheel vehicle: Investigation of wings installation under different speeds," in *Journal of Physics: Conference Series*, 2020, doi: 10.1088/1742-6596/1700/1/012086.

[26] J. D. Kee, J. H. Rho, K. H. Kim, and D. H. Lee, "High speed driving stability of passenger car under crosswind effects," *International Journal of Automotive Technology*, 2014, doi: 10.1007/s12239-014-0077-8.

[27] S. Zou, X. He, and H. Wang, "Numerical investigation on the crosswind effects on a train running on a bridge," *Engineering Applications of Computational Fluid Mechanics*, 2020, doi: 10.1080/19942060.2020.1832920.

[28] T. Tunay, E. Firat, and B. Sahin, "Experimental investigation of the flow around a simplified ground vehicle under effects of the steady crosswind," *International Journal of Heat and Fluid Flow*, 2018, doi: 10.1016/j.ijheatfluidflow.2018.03.020.

[29] L. Liu, Y. Sun, X. Chi, G. Du, and M. Wang, "Transient aerodynamic characteristics of vans overtaking in crosswinds," *Journal of Wind Engineering and Industrial Aerodynamics*, 2017, doi: 10.1016/j.jweia.2017.07.014.

[30] B. Duncan, L. D'Alessio, J. Gargoloff, and A. Alajbegovic, "Vehicle aerodynamics impact of on-road turbulence," *Proceedings of the Institution of Mechanical Engineers, Part D: Journal of Automobile Engineering*, 2017, doi: 10.1177/0954407017699710.

[31] W. Meile, G. Brenn, A. Reppenhagen, B. Lechner, and A. Fuchs, "Experiments and numerical simulations on the aerodynamics of the ahmed body," *CFD Letters*, 2011.

[32] S. R. Ahmed, G. Ramm, and G. Faltin, "Some salient features of the time-averaged ground vehicle wake," in *SAE Technical Papers*, 1984, doi: 10.4271/840300.

[33] D. W. Karmiadji, M. Gozali, M. Setiyo, T. Raja, and T. A. Purnomo, "Comprehensive Analysis of Minibuses Gravity Center: A Post-Production Review for Car Body Industry," *Mechanical Engineering for Society and Industry*, vol. 1, no. 1, pp. 31–40, 2021.